SHOCK-WAVE AND SHEAR-LAYER OSCILLATIONS OVER A DOUBLE CONE IN HIGH-SPEED FLOW

Vaisakh Sasidharan
Department of Aerospace Engineering
Indian Institute of Science
Bengaluru 560012, India
<vaisakhs@iisc.ac.in>

Gaurav Kumar
Department of Aerospace Engineering
Indian Institute of Science
Bengaluru 560012, India
<gauravkumar2@iisc.ac.in>

Akshaya G. Kumara
Department of Aerospace Engineering
Indian Institute of Science
Bengaluru 560012, India
<akshayag@iisc.ac.in>

Subrahmanyam Duvvuri
Department of Aerospace Engineering
Indian Institute of Science
Bengaluru 560012, India
<subrahmanyam@iisc.ac.in>

ABSTRACT

Small-amplitude shock-wave oscillations in a canonical double-cone geometry are investigated by wind tunnel experiments and large-eddy simulation (LES) at Mach 6 flow conditions. The second cone angle is fixed at 90° while the first cone angle and the ratio of the slant heights are varied as parameters. Two distinct type of flow oscillations are observed and characterized using time-resolved schlieren data from the experiments. The Strouhal number for the oscillations is obtained through spectral proper orthogonal decomposition of schlieren data. The LES results, which are found to match well with the experiment, clearly show the three-dimensional nature of flow unsteadiness. Key results from this work and a discussion are presented here.

INTRODUCTION

High-speed flow over a double cone geometry is a canonical problem that exhibits interesting unsteady shear-layer and shock-wave dynamics. A concise account of the general double-cone problem is provided by Hornung *et al.* (2021). Recent experimental work by Sasidharan & Duvvuri (2021) showed two disparate states of shock-wave and flow unsteadiness for a particular class of double-cone geometries where the second-cone angle is fixed at 90°. Here the flow is governed by two geometric parameters – the first cone angle (θ_1) and ratio of slant lengths of the two cones (Λ) – illustrated in figure 1*a*. A certain portion of the two-parameter space (see figure 1*b*) was found to exhibit large-scale shock-wave unsteadiness, termed as *pulsation*, which is driven by periodic unsteady growth and collapse of the separated flow region that forms over the conical surface. Whereas in an other portion, distinct small-amplitude shock-wave oscillation is observed, and this type of unsteadiness is simply termed as *oscillation*. The flow was found to be steady outside the pulsation and oscillation regions. Based on qualitative observations of time-resolved schlieren data, the oscillations were hypothesised as being driven by instabilities in the shear layer that forms over a separated region of the flow (Sasidharan & Duvvuri, 2021).

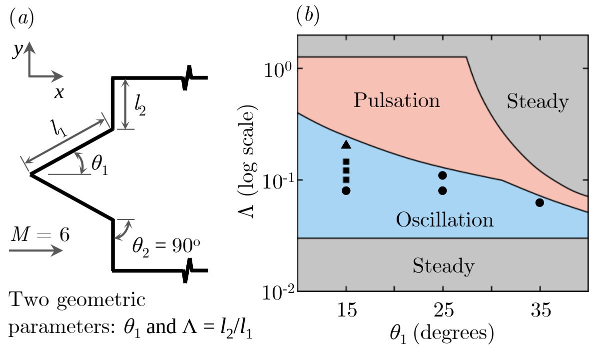

Figure 1. (*a*) A schematic of the axisymmetric double-cone model with $\theta_2 = 90^\circ$. (*b*) θ_1–Λ parameter space with classification of flow states as per Sasidharan & Duvvuri (2021). Data markers in the oscillation regime denote individual experiments from the present work.

The present study is aimed at obtaining a more detailed understanding of the small-amplitude shock-wave oscillations and associated flow unsteadiness. To that end, new experiments and large-eddy simulation (LES) of the flow were performed. Results from these efforts and discussion are presented here.

EXPERIMENTAL AND COMPUTATIONAL SET-UP

Mach 6 flow experiments were performed at IISc in the Roddam Narasimha Hypersonic Wind Tunnel, a 0.5 meter diameter enclosed free-jet facility that uses dry air as the working fluid in a pressure-vacuum mode. The free-stream unit Reynolds number was set to $9.9 \times 10^6\,\mathrm{m}^{-1}$ with stagnation pressure $P_0 = 11.1$ bar and stagnation temperature $T_0 = 455$ K. Axisymmetric double cone models with fixed $\theta_2 = 90^\circ$ were used, with θ_1 and $\Lambda = l_2/l_1$ being varied across experiments such that their range remained restricted to the oscillations regime of the governing parameter space. It is noted that each data marker in figure 1*b* in the oscillation region denotes an individual experiment. In all experiments high-speed schlieren data was acquired with camera framing rates in the range 48,000 to 140,000 frames-per-second with an effective frame exposure time of 10 ns. The total number of frames (or snapshots) in each experiment range from 8000 to 25000. This experimental data provides good spatio-temporal resolution for detailed analysis of flow features.

Large-eddy simulation (LES) of the flow was carried out for a particular combination of $[\theta_1, \Lambda] = [15^\circ, 0.20]$, which corresponds to one of the experimental data points in figure 1*b*, to probe the flow in a more detailed manner than allowed by experimental data. A set of low-pass filtered conservation equations – mass, momentum, energy – are solved using a density-based compressible-flow solver that utilizes an unstructured finite volume formulation in OpenFOAM® (see Kumar & De, 2021; Greenshields, 2018). Flow behavior at the small scales is lumped into a single term in the governing equations (low-wavenumber-pass filtering) and is cast as a turbulent stress tensor. The wall adapting local eddy-viscosity (WALE) model of Nicoud & Ducros (1999) is used at the sub-grid scales to close the turbulent stress tensor term in the numerical simulations. The double cone surface is modelled as an adiabatic no-slip wall with sufficient grid resolution to maintain the average grid size at the wall close to 1 viscous wall unit. The free boundaries away from the surface are modelled as non-reflecting boundaries. The free-stream flow is treated to be uniform with nominally steady velocity, pressure, temperature corresponding to the wind tunnel experiments. The fluctuations in the wind tunnel free-stream are not accounted for in the LES since they are deemed to not have a significant effect on the flow phenomenon that is of present interest. The numerical discretization methods that are used provide an overall 2^{nd} and 3^{rd} order spatial and temporal accuracy respectively in the numerical solution. The time step size for numerical integration of the governing equations is around one nanosecond, and that corresponds to a Courant–Friedrichs–Lewy (CFL) number of 1. The simulation was carried out on a 3D multi-block structured grid with 12 million cells.

RESULTS AND DISCUSSION

Consider the $\theta_1 - \Lambda$ parameter space shown in figure 1*b*. For any fixed θ_1, as Λ is increased starting from $\Lambda = 0$, a separation bubble emerges in the vicinity of the cone base, nested by the corner. The bubble gives rise to a region of flow over it with large shear, *i.e.* a shear layer. The extent of the bubble along the conical surface increases with Λ, thereby leading to longer development lengths for the shear layer. Beyond a certain critical development length, rapid spatial growth of instabilities in the shear layer results in the onset of oscillations. At this point the flow transitions from a steady regime into the oscillations regime. A further increase in Λ, beyond another transition point, moves the flow into the pulsation regime. Here a bow shock wave forms around the shoulder of the second cone and interacts with the leading separation shock wave, and the resulting dynamics bring about a drastic change in the overall flow behavior in comparison to the oscillation state (Sasidharan & Duvvuri, 2021). Since the present focus is on oscillations, flow pulsations are not discussed further.

Figure 2 shows an instantaneous schlieren image of the flow for $[\theta_1, \Lambda] = [25^\circ, 0.11]$ as a representative example of the flow in the state of oscillations. (Note that only the top half of the flow field is shown in all the schlieren images presented here.) The fore-body generates a conical shock wave, which

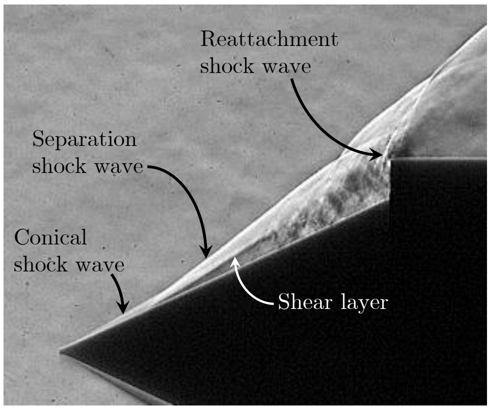

Figure 2. An instantaneous schlieren snapshot of the flow with $[\theta_1, \Lambda] = [25^\circ, 0.11]$.

interacts with the downstream separated flow that is induced by the blunt aft-body. The separated flow generates a shock wave, *i.e.* the separation shock wave, and a shear layer develops between the separated flow region and the supersonic flow over it. A reattachment shock wave is generated at the aft-body as the shear layer impinges the second cone around the shoulder region.

In the present experiments a distinct type of unsteady shock-wave motion associated with oscillations was observed at $\theta_1 = 15^\circ$. For purposes of differentiation from the previously reported oscillation type (Sasidharan & Duvvuri, 2021), this flow state is labeled as "anchored-oscillation." And the previously reported oscillation type is now labeled "free-oscillation." These distinct oscillation types, which are an interesting feature of the flow, are discussed below in detail.

Free- and anchored-oscillations

We consider the case of $[\theta_1, \Lambda] = [15^\circ, 0.08]$ as representative example of free-oscillation. Figures 3*a* and 3*b* show instantaneous schlieren snapshots of this flow at two different time instants in the free-oscillation cycle, separated in time by approximately half a period of oscillation. The point of flow separation, which is also the location of the separation shock wave foot, is marked as 'S' and 'S′' respectively in the two images. From a comparison of the location between 'S' and 'S′', it is straightforward to see that the separation point executes back-and-forth translation along the conical surface. This unsteady motion of the separation point is due to the periodic expansion and contraction in the size/volume of the separation region, which is brought about by the impingement of the unsteady shear layer on the second cone. The key features of free-oscillation are schematically illustrated in figure 3*c*, where the extreme locations of the separation point within one cycle are labeled 'S' and 'S′'. The periodic motion of the separation point is seen to also bring about a continuous back-and-forth shift in the spatial location where instabilities in the shear layer begin to manifest. This location is identified a '×' marker and labeled 'T' and 'T′' in figures 3*a* and 3*b* respectively. From the schlieren images it is noted that flow disturbances arising from the shear layer instability interact with the separation shock wave and bring about undulations in its structure. Experiments in which free-oscillations were observed are indicated by a '•' marker in figure 1*b*.

Anchored-oscillation flow state was observed for $[\theta_1, \Lambda] = [15^\circ, 0.20]$; this location in the parameter space is marked by a '▲' marker in figure 1*b*. Figures 4*a* and 4*b* show

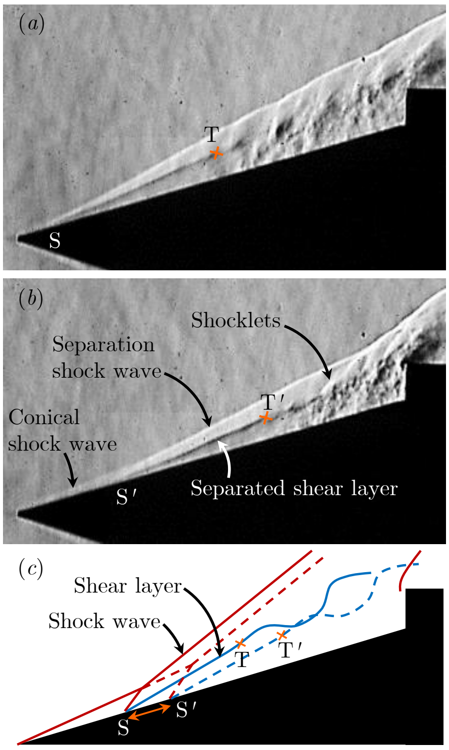

Figure 3. (*a*) and (*b*): Schlieren snapshots at two different time instants within a cycle of free-oscillation for $[\theta_1, \Lambda] = [15^\circ, 0.08]$. (*c*) A schematic illustration of free-oscillations.

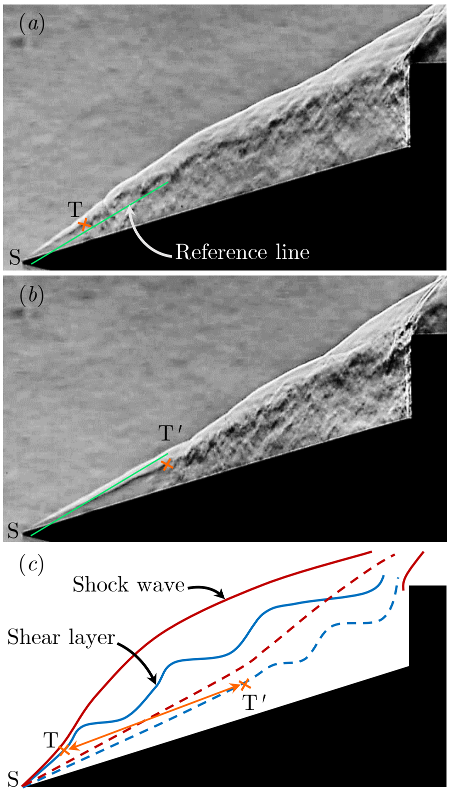

Figure 4. (*a*) and (*b*): Schlieren snapshots at two different time instants within a cycle of anchored-oscillation for $[\theta_1, \Lambda] = [15^\circ, 0.20]$. (*c*) A schematic illustration of anchored-oscillations.

instantaneous schlieren snapshots of the flow at two different time instants in the anchored-oscillation cycle, separated in time by approximately half a period of oscillation. At this larger Λ (relative to free-oscillation case discussed above), the separation bubble envelopes the entire cone surface. With that the separation point 'S' is pushed to cone nose and remains anchored at that location throughout the entire oscillation cycle. The periodic expansion/contraction cycles of the separation bubble lead to a larger scale distortion in the separation shock wave structure, in comparison with free-oscillation. The overall motion of the separation shock-wave traces out an approximately bi-convex shape; this aspect is schematically illustrated in figure 4*c*. Local undulations in the shock-wave structure that are induced by shear layer disturbances accompany the larger scale coherent motion. Significant variation in the local angle (inclination) of the separation shock wave near the cone nose brings about unsteady variation in the downstream shear layer Mach number distribution. This is expected to continually alter the shear layer stability characteristics. Direct evidence for the same is seen in the schlieren images where the location of 'T' (marked by '×') shows significant displacement. This is perhaps an important aspect of the mechanism that sustains the overall flow unsteadiness.

While only the free-oscillation flow state was found for $\theta_1 = 35^\circ$ and $\theta_1 = 25^\circ$, a reduction in θ_1 to 15° revealed the distinct anchored-oscillation flow state at sufficiently large Λ. Hence, in the $\theta_1 - \Lambda$ parameter space the first appearance of anchored-oscillations with reducing θ_1 is expected to occur at some θ_1 between 25° and 15°. Another interesting flow feature observed at $\theta_1 = 15^\circ$ is the blurred nature of the boundary between free- and anchored-oscillations as Λ is increased from 0.08 (figure 3) to 0.20 (figure 4). Flows at the three experimental data points between Λ of 0.08 and 0.20, marked by '▪' in figure 1*b* (Λ values of 0.10, 0.12, 0.14), displayed a mix of features described above for free- and anchored-oscillation states. The primary observation at these three values of Λ is that the separation point 'S' remains anchored at the nose for only a portion of the oscillation cycle, and translates along the cone surface for the remaining cycle duration.

Strouhal number scaling

Following the characterization of physical features, we seek to now extract a timescale and associated spatial structure for oscillations. The modal decomposition technique of spectral proper orthogonal decomposition (SPOD; see Towne *et al.*, 2018) is applied to the schlieren dataset. SPOD is a frequency-domain variant of the conventional proper orthogonal decomposition (POD) technique, and is well suited for extracting spatio-temporal coherent structures in statistically stationary flows. An ensemble of realisations of schlieren intensity field $q(\mathbf{x},t) = \{q_j(\mathbf{x},t), j = 1,2,\ldots,n\}$, where n, $\mathbf{x}$, and t are the total number of realizations, spatial coordinate vector, and time respectively, is first transformed to power spectral density (PSD) field $\hat{q}(\mathbf{x},f) = \{\hat{q}_j(\mathbf{x},f), j = 1,2,\ldots,n\}$ in the frequency (f) domain. Subsequently, $\hat{q}(\mathbf{x},f)$ is decomposed into orthogonal modes at individual frequencies through POD:

$$\hat{Q}(\mathbf{x},f) = \sum_{j=1}^{n} a_j(f)\psi_j(\mathbf{x},f). \tag{1}$$

This essentially means that SPOD decomposes the ensemble of realisations $\hat{q}(\mathbf{x},f)$ into orthogonal modes $\psi_j(\mathbf{x},f)$ at different frequencies, and $\hat{Q}(\mathbf{x},f)$ represents the optimal recon-

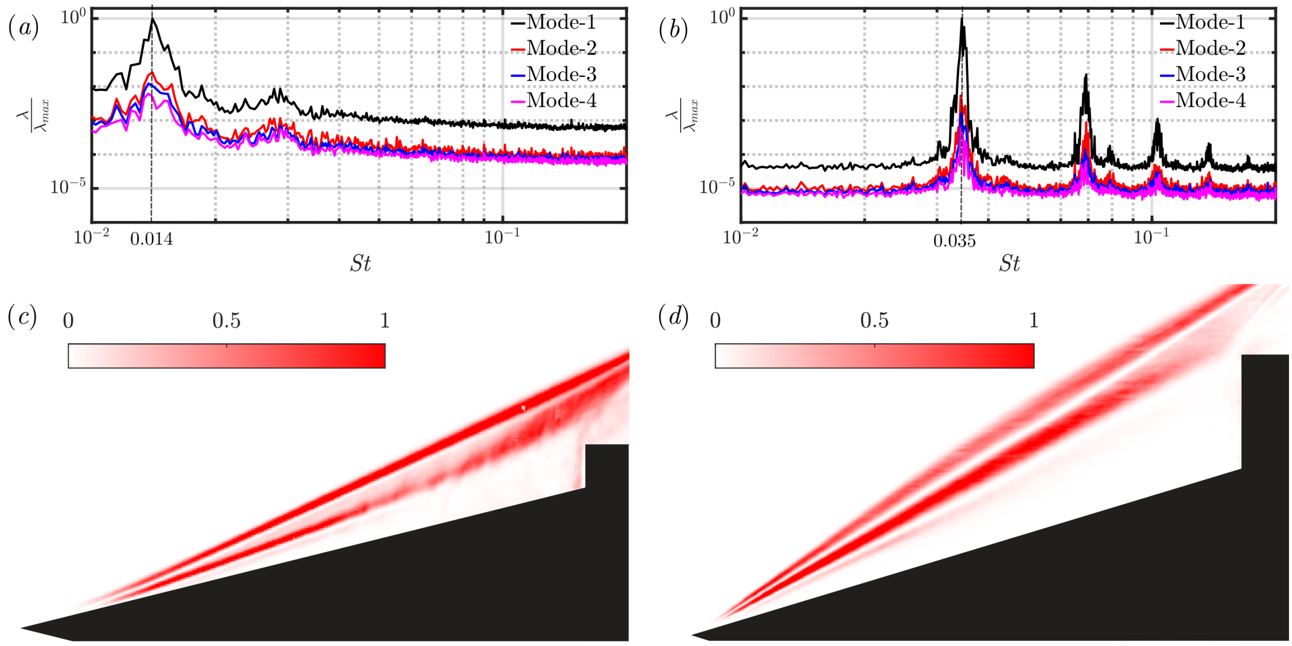

Figure 5. Modal energy spectra from SPOD normalized by maximum energy of the leading mode (top row) and the corresponding mode shape of the leading mode (bottom row). (*a*, *c*) Free-oscillation for $\theta_1 = 15^\circ$ and $\Lambda = 0.08$. (*b*, *d*) Anchored-oscillation for $\theta_1 = 15^\circ$ and $\Lambda = 0.20$.

struction of the flow data set that contains the maximum energy (variance) of the ensemble. This optimization problem leads to an eigen value decomposition problem, and the eigen values corresponding to these modes at different frequencies are represented by $\lambda_j(f) = a_j^2(f)$. With the present data set, PSD of the schlieren snapshot matrix was calculated to obtain convergent estimates of spectral density as per the recommendation of Towne *et al.* (2018). The SPOD modes are ranked based on the corresponding λ_j values, and then the leading mode can represent the dominant coherent structure in the flow.

Figure 5 shows SPOD results for the two specific oscillation cases discussed in the previous section. In both flow scenarios the leading mode is seen to be much more energetic in comparison with the other modes, and hence it provides a good representation of any coherent spatial structure present in the flow. A peak in the spectra can be clearly identified in both cases, which indicates the presence of a dominant time scale that characterizes flow unsteadiness, *i.e.* a frequency for oscillations. Non-dimensional frequency *St* (Strouhal number) is defined here as

$$St = \frac{f l_2}{U_\infty}, \tag{2}$$

where U_∞ is the free-stream velocity. From the spectra plots the Strouhal numbers for these free- and anchored-oscillations cases are inferred to be 0.014 and 0.035 respectively. SPOD analysis outlined here was also performed for the rest of the data points shown in figure 1. The results are summarized in figure 6 in the form of a Strouhal number plot.

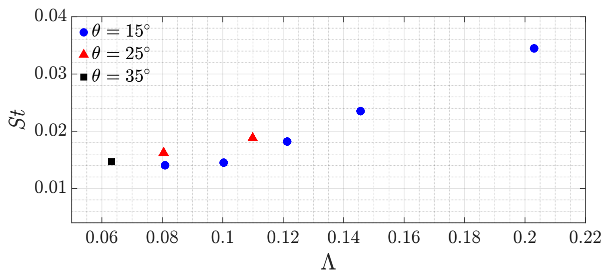

Figure 6. The Strouhal number (*St*) defined based on dominant frequency (f) obtained from SPOD for the $\theta_1 - \Lambda$ parameter space exhibiting oscillations.

3D nature of flow unsteadiness

The results of LES that was carried out for the case $[\theta_1, \Lambda] = [15^\circ, 0.20]$ are discussed here. As seen above, this combination of θ_1 and Λ results in anchored-oscillations. Figure 7 shows a qualitative comparison between experimental and synthetic schlieren images from LES at four different instances within one oscillation time period (T). Phase locking between the experimental and computational data was done simply by visual assessment. From the figure it is seen that the location/shape of shear layer and shock wave are captured by the LES with reasonable accuracy (with reference to the experiment). It is noted that the synthetic schlieren was generated using vertical-direction density gradients on a single azimuthal plane, *i.e* a 2D slice of 3D data. Whereas the experimental schlieren contains artefacts of flow non-uniformity along the span (direction of schlieren light beam propagation). Hence a close match between the two is not expected. For quantitative validation of the LES, static pressure p is probed at six different locations in an azimuthal plane. These locations, which are marked in figure 8, are in the separation bubble and shear layer regions of the flow. All the PSD curves of static pressure in figure 8 clearly show a peak at $St = 0.035$, which matches very well with the value obtained from the corresponding experiment.

LES data allows for a detailed inspection of the 3D flow field. Figure 9*a* shows a 3D visualization of instantaneous streamwise-direction density gradient in the flow. Figures 9*b* to 9*e* show the same data at four different planes normal to the

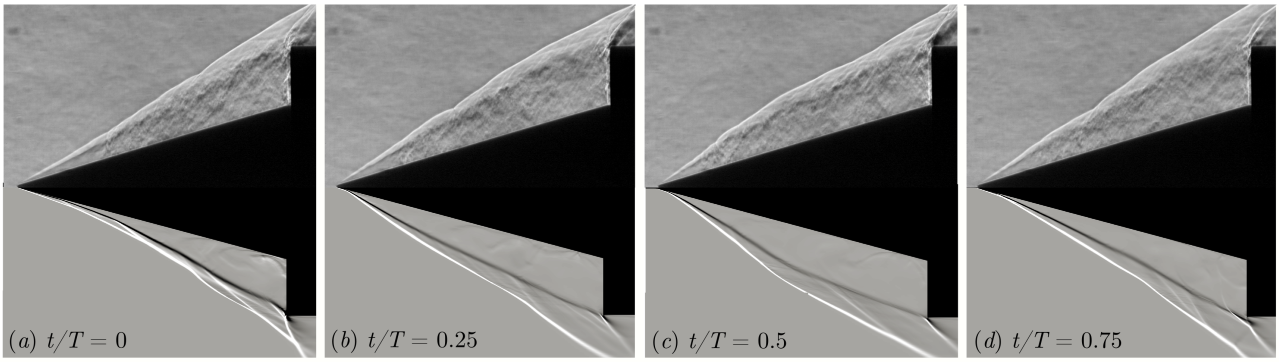

Figure 7. Comparison between the experimental (top half of images) and synthetic (bottom half of images) schlieren images from LES for a double cone configuration with $\theta_1 = 15°$ and $\Lambda = 0.20$ at four different time (t) instances within an oscillation time period (T). The position/shape of the separation shock wave and the shear layer are qualitatively similar. A quantitative match is found between the two for the oscillation time period.

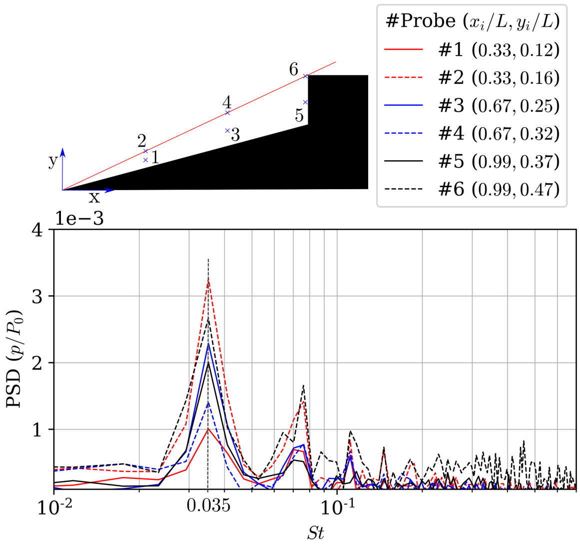

Figure 8. Power spectral density (PSD) of non-dimensional pressure (p/P_0) obtained from LES for $\theta_1 = 15°$ and $\Lambda = 0.20$ at six different probe locations (marked at the top). The probes are placed at three equally-spaced streamwise planes x_i/L = 0.33, 0.67, 0.99. Here $L = l_1 \cos\theta_1$.

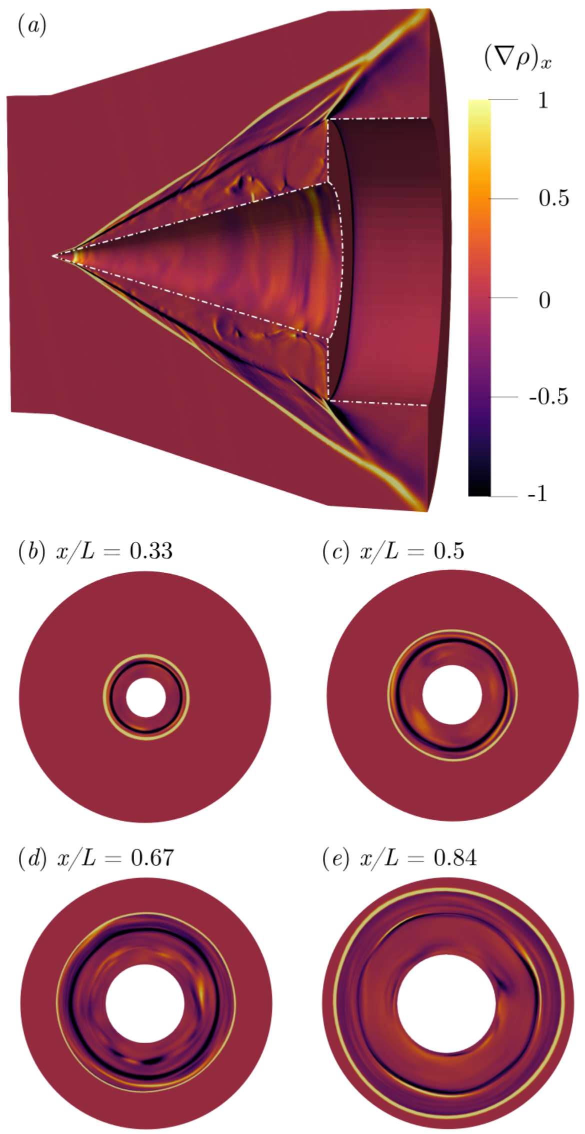

Figure 9. A visualization of instantaneous streamwise-direction density gradient (normalized) generated from LES data $\theta_1 = 15°$ and $\Lambda = 0.20$. (*a*) Azimuthal plane cut-away view. (*b-e*) Sectional views at four different streamwise planes. Here $x = 0$ is cone nose and $L = l_1 \cos\theta_1$.

streamwise direction, centered on the cone axis. The three-dimensional nature of unsteadiness in the flow is evident from a visual inspection of the figure; density-gradient iso-contours reveal clear azimuthal variation in the flow structure. These results indicate that any stability analysis of the flow aimed at explaining the oscillation phenomenon will be required to account for non-zero wavenumbers in the azimuthal direction.

BRIEF CONCLUSIONS

Shock-wave oscillations were investigated in a double-cone geometry with $\theta_2 = 90°$. Experimental data revealed two distinct types of oscillations, and they were termed as free- and anchored-oscillations. The latter oscillation type has not been previously reported, and calls for further investigation. Present data suggests that the region of the θ_1–Λ parameter space that supports anchored-oscillations would grow with reducing θ_1, *i.e.* the boundaries of the anchored-oscillation regime would span a larger range of Λ at lower θ_1. SPOD analysis shows that both oscillation types can be described by a dominant time scale. LES was performed for a particular combination of θ_1 and Λ where the flow exhibits anchored-oscillation, and the oscillation time scale obtained from it matched well with experimental results. The simulation results clearly showed the three-dimensional nature of flow unsteadiness. LES data will be probed further to understand the physical behavior of the separation bubble and the shear layer, with a view toward developing a mechanistic model to explain the oscillation phenomenon.

ACKNOWLEDGEMENTS

Support from SERB National Postdoctoral Fellowship (V.S. – file no. PDF/2020/001278; G.K. – file no. PDF/2021/001358), GoI Ministry of Education MTech Scholarship (A.G.K.), and Saroj Poddar Trust (S.D.) is gratefully acknowledged.

REFERENCES

Greenshields, C. J. 2018 Openfoam user guide version 6. *The OpenFOAM Foundation* p. 237.

Hornung, H. G., Gollan, R. J. & Jacobs, P. A. 2021 Unsteadiness boundaries in supersonic flow over double cones. *Journal of Fluid Mechanics* **916**, A5.

Kumar, G. & De, A. 2021 Modes of unsteadiness in shock wave and separation region interaction in hypersonic flow over a double wedge geometry. *Physics of Fluids* **33** (7), 076107.

Nicoud, F. & Ducros, F. 1999 Subgrid-scale stress modelling based on the square of the velocity gradient tensor. *Flow, Turbulence and Combustion* **62** (3), 183–200.

Sasidharan, V. & Duvvuri, S. 2021 Large- and small-amplitude shock-wave oscillations over axisymmetric bodies in high-speed flow. *Journal of Fluid Mechanics* **913**, R7.

Towne, A., Schmidt, O. T. & Colonius, T. 2018 Spectral proper orthogonal decomposition and its relationship to dynamic mode decomposition and resolvent analysis. *Journal of Fluid Mechanics* **847**, 821–867.